Inorganica Chimica Acta 483 (2018) 571–578

Contents lists available at ScienceDirect

Inorganica Chimica Acta

journal homepage: www.elsevier.com/locate/ica

Research paper

Mitochondria localizing high-spin iron complexes of curcumin for photo-induced drug release

Avishek Jana[a], Brijesh K. Verma[b], Aditya Garai[a], Paturu Kondaiah[b,*], Akhil R. Chakravarty[a,*]

[a] Department of Inorganic and Physical Chemistry, Indian Institute of Science, Sir C V Raman Avenue, Bangalore 560012, India
[b] Department of Molecular Reproduction, Development and Genetics, Indian Institute of Science, Sir C V Raman Avenue, Bangalore 560012, India

ARTICLE INFO

Keywords:
Bioinorganic chemistry
Iron
Curcumin
Mitochondrial localization
Drug photo-release
DNA cleavage

ABSTRACT

High-spin iron complexes $[Fe^{II}(L^1)(cur)]Cl$ (**1**), $[Fe^{III}(L^2)(cur)]Cl$ (**2**) and $[Fe^{III}(L^3)(cur)]$ (**3**), where L^1 is tris(2-pyridylmethyl)amine, HL^2 is N,*N*-bis(2-pyridylmethyl)-N-(2-hydroxybenzyl)amine and H_2L^3 is N,*N*-dimethyl-N',N'-bis(4,6-ditertiarybutyl-2-hydroxybenzyl)ethylenediamine and Hcur is curcumin, were synthesized, characterized and their redox-mediated and/or visible light induced release of curcumin, photo-induced DNA cleavage and anticancer activity studied. The molecular structures of **1–3** were optimized from DFT (density functional theory) calculations. The $t_{2g}^3e_g^2$-iron(III) complexes showed a curcumin based electronic spectral band at ~ 425 nm in 1:1 DMF/DPBS (Dulbecco's phosphate-buffered saline) and displayed the Fe(III)-Fe(II) redox couple near −0.36 V vs. SCE (saturated calomel electrode) in DMF-0.1 M TBAP (tetrabutylammonium perchlorate). The complexes are avid binders to calf thymus DNA. Complex **1** showed photo-cleavage of pUC19 DNA in visible light of 446 nm forming $^{\cdot}OH$ radicals as the reactive oxygen species. The complexes as curcumin carrier showed photo-cytotoxicity in different cell lines on visible light activation. Imaging study showed their subcellular mitochondrial localization.

1. Introduction

An important aspect in the chemistry of metal-based anticancer agents is their delivery to the targeted cancer cells [1–3]. The chemotherapeutic drugs like cisplatin and its analogues as transcription inhibitors are known to suffer from their reduced efficacy and dose limited toxicity due to their non-selective properties [4–7]. Curcumin (Hcur), as an active component of the natural product turmeric, is well known for its cellular activity by preventing tumor progression and inhibiting angiogenesis in cultured endothelial vascular cells and in animal models [8–12]. It induces apoptosis via mitochondrial pathways involving caspases and Bcl-2 family of proteins. It also interferes with the activity of the transcription factor NF-κB which is known to enhance the activity of the tumor suppressor protein p53. Curcumin as a photoactive molecule is known to display photo-cytotoxicity causing cell shrinkage, membrane blebbing and apoptosis indicating its potential as a photosensitizer and chemotherapeutic agent [13,14]. The major drawback of curcumin is its extremely rapid metabolism in the cellular medium and poor aqueous solubility thus severely reducing its bioavailability and overall efficacy when compared to those of cisplatin [15,16]. A daily dose of ~10 g of curcumin gives a plasma concentration of less than 1.0 mg mL^{-1}. The current approaches to improve the pharmacokinetics of curcumin are based on (i) to alter its structural features resulting in more soluble analogues and conjugates or (ii) encapsulation of curcumin in nanoparticle formulations such as liposomes, micelles, and phospholipids [17–19]. A large number of synthetic curcuminoids were prepared with an aim to overcome the limitations [20]. Lipid vesicles, nanoparticles, and nanofibers are used as delivery systems to augment the bioavailability of curcumin, but this methodology limits the therapeutic window and leads to off-target toxicity [16]. A more innovative strategy, as we feel, is to stabilize curcumin on binding to a bio-friendly transition metal ion, namely iron, using the enolic tautomeric form of the dye [21–26].

We have chosen iron for this very purpose considering the oxophilicity and bio-essential nature of iron which with its rich coordination chemistry is very important for human health. The well-known clinically successful anticancer antibiotic drug of this metal is iron-bleomycin (Fe-BLM) which is a metalloglycopeptide [27]. Iron in its trivalent oxidation state forms stable chelates as catecholates and hydroxamates as found in siderophores and enterobactins [28,29]. Such ligands have, however, reduced binding affinity to the same metal in its bivalent oxidation state. An alteration of the redox state promotes the facile release of the oxygen-donor ligands as is known for enterobactin and transferrin. Keeping that in mind, new iron complexes with the

* Corresponding authors.
E-mail addresses: paturu@iisc.ac.in (P. Kondaiah), arc@iisc.ac.in (A.R. Chakravarty).

https://doi.org/10.1016/j.ica.2018.09.008
Received 27 June 2018; Received in revised form 3 September 2018; Accepted 4 September 2018
Available online 05 September 2018

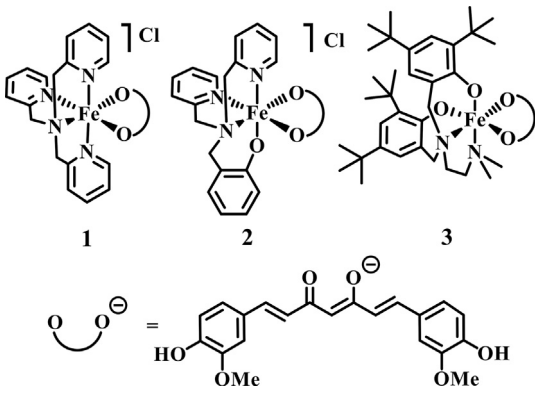

Fig. 1. Schematic drawing of the iron complexes **1–3** and the ligands used.

metal in +2 and +3 oxidation states are designed and prepared in this work in which curcumin in its monoanionic O,O-donor enolic form binds to the metal. The objective is to release curcumin by chemical and/or photochemical means from the iron center that is additionally bound to different tetradentate ancillary ligands. Three ligands are chosen with NNNN (L^1), NNNO (HL^2) and NNOO (H_2L^3) donor atoms to alter the physicochemical properties of the complexes. Herein, we present the high-spin iron(II) and iron(III) complexes, namely, $[Fe^{II}(L^1)(cur)]Cl$ (**1**), $[Fe^{III}(L^2)(cur)]Cl$ (**2**) and $[Fe^{III}(L^3)(cur)]$ (**3**), where L^1 is tris(2-pyridylmethyl)amine, HL^2 is N,*N*-bis(2-pyridylmethyl)-N-(2-hydroxybenzyl)amine, H_2L^3 is N,*N*-dimethyl-N',N'-bis(4,6-ditertiarybutyl-2-hydroxybenzyl)ethylenediamine and Hcur is curcumin (Fig. 1). While complex **1** has iron in its +2 oxidation state, complexes **2** and **3** have the ferric ion. The effect of oxidation state of the metal and the effect of donor atoms on the stability of the complexes relative to free curcumin and comparative curcumin release kinetics are studied with an aim to achieve a structure activity relationship (SAR). In addition, the DNA photocleavage and visible light-induced anticancer activity of the complexes are studied.

Curcumin has rich photophysical and photochemical properties. It has an absorption spectral band within 410–430 nm and a fluorescence spectral band within 460–560 nm in different solvents and in transition metal complexes [30]. Curcumin as a photosensitizer is thus potentially suitable for photo-chemotherapeutic applications [31]. The fluorescent property of curcumin complexes emitting in green is suitable for cellular imaging study to ascertain any subcellular localization of the complexes. The photosensitizing property of curcumin is used to study the light-induced anticancer activity of the iron complexes **1–3**. The significant results of this study include observation of photo-induced cellular release of the iron bound curcumin dye as a potential photo-chemotherapeutic agent, predominant mitochondrial localization of the complexes showing photo-cytotoxicity in visible light (400–700 nm) and photo-induced cell death forming reactive oxygen species (ROS).

2. Experimental

2.1. Materials

All the reagents and chemicals were procured from commercial sources (S. D. Fine Chemicals, India; Sigma-Aldrich, U.S.A.) and used as such without any further purification. The solvents were purified by standard reported procedures [32]. Tris[(2-pyridyl)methyl] amine (L^1), N,*N*-bis(2-pyridylmethyl)-N-(2- hydroxybenzyl)amine (HL^2) and N,*N*-dimethyl-Ń,Ń-bis(4,6-ditertiarybutyl-2-hydroxybenzyl)ethylenediamine (H_2L^3) were prepared following literature procedures [33–35]. Syntheses of the complexes were carried out under nitrogen atmosphere using standard Schlenk technique. Supercoiled (SC) pUC19 DNA was purchased from Bangalore Genie (India). Curcumin (Hcur), 2-picolylamine, calf thymus (ct) DNA, agarose (molecular biology grade), catalase, superoxide dismutase (SOD), 2,2,6,6-tetramethyl-4-piperidone (TEMP), Hoechst 33,258 (bis-benzimidazole derivative), distamycin, methyl green, MTT (3-(4,5-dimethylthiazole-2-yl)-2,5-diphenyltetrazolium bromide) and ethidium bromide (EB) were purchased from Sigma-Aldrich (USA). Tris(hydroxymethyl)aminomethane-HCl (Tris-HCl) buffer solution was prepared using deionized and double-distilled water.

2.2. General methods

The elemental analyses were performed on Thermo Finnigan Flash EA 1112 analyser. Electrospray ionization mass spectral measurements were done using Esquire 3000 plus ESI (Bruker Daltonics) and Q-TOF Mass spectrometers. ^{1}H NMR spectral measurements were made using a Bruker 400 MHz NMR spectrometer. The FT infrared and UV–visible spectra were recorded using Bruker Alpha and PerkinElmer Spectrum 650 spectrophotometers respectively. Emission spectral measurements were carried out with a PerkinElmer LS 55 spectrophotometer. Cyclic voltammetric measurements were made at 25 °C on a EG&G PAR Model 253 VersaStat potentiostat/galvanostat with an electrochemical analysis software 270 using a three electrode set up comprising a platinum working electrode, a platinum wire auxiliary electrode and a saturated calomel reference (SCE) electrode. Tetrabutylammonium perchlorate (TBAP, 0.1 M) was used as a supporting electrolyte in dimethylformamide (DMF). The electrochemical data were uncorrected for junction potential. Tetrabutylammonium perchlorate (TBAP) was prepared with caution by drop-wise addition of perchloric acid to a tetrabutylammonium bromide solution in water with vigorous stirring followed by filtration of the white solid and thorough washing with water to remove the acid. Necessary care was taken in handling TBAP due to its explosive nature. Conductivity measurements were done using a Control Dynamics (India) conductivity meter using 1.0 mM solution of the complexes in DMF and 1:1 (v/v) aqueous DMF. Magnetic susceptibility measurements at 298 K were done using dry powdered samples of the complexes using a magnetic susceptibility balance from Sherwood Scientific (Cambridge, U.K.) and $Hg[Co^{II}(SCN)_4]$ as a standard.

2.3. Synthesis of the complexes *1–3*

The complexes were synthesized by following a common procedure. For iron(II) complex $[Fe(L^1)(cur)]Cl$ (**1**), a solution of ligand L^1 (0.87 g, 3 mmol) in 2 mL MeOH was added drop-wise to a solution of anhydrous $FeCl_2$ (0.38 g, 3 mmol) in 3 mL MeOH. The resulting solution was stirred at 25 °C under N_2 atmosphere for 1 h. A slow evaporation of the solvent gave a dark brown solid which was washed with hexane. The solid (0.83 g, 2 mmol) was dissolved in 3 mL MeOH and a solution of curcumin (Hcur, 0.73 g, 2 mmol) in 5 mL CH_2Cl_2:MeOH (1:1 v/v), previously deprotonated by NEt_3 (0.2 g, 2 mmol), was added drop-wise to this with stirring at 25 °C under N_2 for 3 h. Solvent was evaporated from the resulting dark red solution by slow evaporation and a dark brown solid was isolated, washed with diethyl ether and cold MeOH and finally dried in vacuo over P_2O_5 to obtain complex **1** in analytically pure form.

For the iron(III) complex $[Fe(L^2)(cur)]Cl$ (**2**), a solution of HL^2 (0.92 g, 3 mmol) in 2 mL MeOH, previously deprotonated with NEt_3 (0.3 g, 3 mmol), was added drop-wise to an anhydrous solution of $FeCl_3$ (0.48 g, 3 mmol) in 3 mL MeOH at 25 °C under N_2 for 1 h. The solution was filtered to get a dark blue solid which was isolated and washed with hexane. The blue solid (0.86 g, 2 mmol) was dissolved in 10 mL MeOH and to this was added drop-wise a solution of Hcur (0.73 g, 2 mmol) in 10 mL CH_2Cl_2:MeOH (1:1), previously treated with NEt_3 (0.2 g, 2 mmol), and the mixture was stirred at 25° C under nitrogen atmosphere for 3 h. Slow evaporation of the solution gave a dark brown solid of complex **2** which was isolated, washed with diethyl ether and hexane before drying in vacuum. For the iron(III) complex **3**, H_2L^3 (1.57 g,

3 mmol) was dissolved in 3 mL CH_2Cl_2 and deprotonated by NEt_3 (0.9 g, 9 mmol). Following the same reaction steps as for complex **2**, a solid was obtained first and a dark red solution in the second step which gave a solid on slow evaporation of the solvent. The product was isolated, washed with diethyl ether and hexane to obtain a dark brown solid of complex **3**.

2.3.1. [Fe(L^1)(cur)]Cl (1)

Yield: 75%. Anal. Calcd for $C_{39}H_{37}N_4O_6ClFe$: C, 62.54; H, 4.98; N, 7.48. Found: C, 62.28; H, 5.02; N, 7.27. Molar conductivity (Λ_M) in DMF (dimethylformamide): 58 S m^2 M^{-1}. FT-IR [solid phase, (cm^{-1})]: 2936 s, 1593 s, 1485 s, 1383 s, 1268 s, 1152 s, 1130 s, 979 m, 820 w, 965 w, 762 w, 455 w (s, strong; m, medium, w, weak). ESI-MS in MeCN (*m/z*): 713.2059 $[M-Cl]^+$. UV–Visible in 1:1 DMF/DPBS buffer [λ_{max}, nm (ε, M^{-1} cm^{-1})]: 315 (17 200), 410 (33 700), 501 (19 200). Emission in DMSO (dimethyl sulfoxide) [λ_{em}, nm]: 530 (Φ_F = 0.02).

2.3.2. [Fe(L^2)(cur)]Cl (2)

Yield: 72%. Anal. Calcd for $C_{40}H_{37}N_3O_7ClFe$: C, 62.96; H, 4.89; N, 5.51. Found: C, 62.79; H, 4.84; N, 5.76. Λ_M in DMF: 56 S m^2 M^{-1}. FT-IR [solid phase, (cm^{-1})]: 2951 s, 1593 s, 1478 s, 1460 s, 1377 s, 1275 s, 1210 s, 1159 s, 1116 s, 968 m, 871 m, 762 w, 459 w. ESI-MS in MeOH (*m/z*): 727.1981 $[M-Cl]^+$. UV-Visible in 1:1 DMF/DPBS buffer [λ_{max}, nm (ε, M^{-1} cm^{-1})]: 428 (22 200), 508 (11 100). Emission in DMSO [λ_{em}, nm]: 527 (Φ_F = 0.03).

2.3.3. [Fe(L^3)(cur)] (3)

Yield: 65%. Anal. Calcd for $C_{55}H_{73}N_2O_8Fe$: C, 69.83; H, 7.78; N, 2.96. Found: C, 69.75; H, 7.45; N, 3.25. Λ_M in DMF: 3 S m^2 M^{-1}. FT-IR [solid phase, (cm^{-1})]: 2951 s, 1593 s, 1492 s, 1356 s, 1290 s, 1217 s, 1152 s, 979 m, 820 m, 466 w. ESI-MS in MeOH (*m/z*): 968.4618 $[M+Na]^+$. UV–Visible in 1:1 DMF/DPBS buffer [λ_{max}, nm (ε, M^{-1} cm^{-1})]: 278 (12 300), 425 (17 960), 513 (7060). Emission in DMSO [λ_{em}, nm]: 526 (Φ_F = 0.02).

2.4. Solubility and stability

The complexes were soluble in solvents such as methanol, ethanol, dimethylformamide and dimethyl sulfoxide. They were less soluble in water, acetonitrile and halogenated solvents, namely, chloroform and dichloromethane. Complexes **1** and **2** were insoluble in hydrocarbons like hexane, petroleum ether but the non-electrolytic complex **3** showed some extent of solubility in these solvents. Complex **1** showed degradation over a period of ~3 weeks of time when kept in the solid state. Complexes **2** and **3** were, however, stable in the solid state and in solution phase in dark. The solution stability of the complexes **1–3** was studied by electronic spectroscopy using their 1:1 DMSO/Tris-HCl buffer solutions.

2.5. Theoretical study

The geometries of the complexes **1–3** were optimized by density functional theory (DFT) using the B3LYP level of theory and LanL2DZ basis set for the iron center and the 6-311G + (d,p) basis set for all other atoms as implemented in the Gaussian 09 program [36,37]. Conductor-like Polarizable Continuum Model (CPCM) was used to model solvation effects with DMSO as solvent. The electronic transitions with their transition probability were obtained using linear response time dependent density functional theory (TDDFT). The geometry of the complexes in the excited state was optimized to get insights into any changes in the structural features. The coordinates of the energy-minimized structures are listed as supporting information data (vide Appendix A).

2.6. Photocytotoxicity experiments

The photo-induced cytotoxicity of the complexes was studied using 3-(4,5-dimethylthiazol-2-yl)-2,5-diphenyltetrazolium bromide (MTT) assay [38]. The estimation of the number of viable cells was obtained from the level of the formazan formed. About 1.0×10^4 human breast carcinomas (MCF-7), human glioblastoma (LN-229) and spontaneously immortalized human keratinocyte (HaCaT) cells were plated separately in 96 well plate in DMEM containing 10% FBS. After 24 h of incubation at 37 °C in a CO_2 incubator, different concentrations of the complexes dissolved in 1% DMSO were added to the cells and incubation was continued for a period of 4 h in dark. The medium was subsequently replaced with phosphate buffered saline (PBS) and cells were photo-irradiated with visible light (400–700 nm) for 1 h using a Luzchem Photoreactor (Model LZC-1, Ontario, Canada) fitted with Sylvania make 8 fluorescent white tubes with a fluence rate of 2.4 mW cm^{-2} to provide a total light dose of 10 J cm^{-2}. Post irradiation, PBS was replaced with DMEM-FBS (FBS, fetal bovine serum) and incubation was continued for a further period of 16 h in dark. After incubation, 25 μL of 4 mg mL^{-1} of MTT was added to each well and incubated for an additional 3 h. After discarding the culture medium, 150 μL of DMSO was added to dissolve the formazan crystals. The absorbance at 570 nm was measured using a BIORAD ELISA plate reader. Cytotoxicity of the test compounds was determined as the percentage ratio of the absorbance of the treated cells to the untreated controls. The IC_{50} values were determined by nonlinear regression analysis (GraphPad Prism 6).

2.7. Confocal microscopy imaging

The localization of the fluorescent complexes in HaCaT cells was visualized using a confocal microscope. The cells were plated on glass cover slips in each 12 well plate at a seeding density of 1.0×10^4 cells. Cells were then incubated with 15 μM of the complexes **1–3** in dark for 4 h period, fixed with 4% formaldehyde for 10 min at 25 °C and washed with PBS. Permeabilization of cells was performed with chilled methanol for 10 min at −20 °C followed by incubation with Hoechst and Mito-Tracker Deep Red FM (MTR) staining solution for 30 min in two different set of experiments. Cells were washed to make them free of excess staining dye and mounted. Images were acquired using a confocal laser scanning microscope (Leica TCS SP5) and analysed using ImageJ image processing software.

2.8. DNA binding experiments

The DNA binding experiments were performed in Tris–HCl buffer (5 mM, pH 7.2) using DMF solution of the complexes **1–3** and calf thymus DNA (ct-DNA) at an ambient temperature. Absorption titration experiments were carried out by varying the concentration of the ct-DNA while keeping the complex concentration as constant. The DNA was found to be free of any protein impurity, as evidenced from the ratio of the absorbance values of the DNA at 260 and 280 nm in Tris-HCl buffer as 1.9:1. Concentration of the DNA was measured from its absorption intensity at 260 nm using ε value of 6600 M^{-1} cm^{-1}. In UV–visible absorption titration, Tris-HCl buffer was used and the concentration of ct-DNA and the complex were in the range of 150–200 μM and 20 μM, respectively. The complex solution was titrated with the DNA, and the absorbance of the band of the complexes at λ_{max} was monitored. To cancel the effect of the DNA absorption, equal quantities of DNA were added into the reference solution during the titration. The intrinsic binding constant (K_b) of the complexes were obtained by using the expression: $[DNA]/(\varepsilon_a - \varepsilon_f) = [DNA]/(\varepsilon_b - \varepsilon_f) + 1/K_b(\varepsilon_b - \varepsilon_f)$, where [DNA] is the concentration of DNA in base pairs, ε_f, ε_a and ε_b are the molar extinction-coefficient values of the free complex in solution, complex bound to DNA at a definite concentration, and the complex in completely DNA bound form, respectively [39,40]. Each set of data upon fitting in the above equation gave a straight line with a slope of 1/

($\varepsilon_b - \varepsilon_f$) and y axis intercept of $1/K_b(\varepsilon_b - \varepsilon_f)$. K_b was determined from the ratio of the slope to the intercept. The linear fitting analysis was done using OriginPro 8.5.

2.9. DNA cleavage experiments

Photo-induced cleavage of supercoiled (SC) plasmid pUC19 DNA (30 μM, 0.2 μg, 2686 base-pairs) and the chemical nuclease activity of the complexes **1–3** in DMF-Tris-HCl buffer (pH 7.2) was studied by agarose gel electrophoresis. Photo-irradiation was accomplished using visible light of 446 nm wavelength from a diode laser (BLM447TA-100 from Shanghai Laser & optics Century Co. Ltd.) of 50 mW laser power. The experiments were performed in a total volume of 20 μL containing supercoiled (SC) DNA (1 μL, 30 μM) and the complexes (20 μM) in a 50 mM Tris-HCl buffer (pH 7.2) containing 50 mM NaCl. All the samples were incubated at 37 °C for one hour prior to irradiation. The samples were exposed to light and incubated for one hour at 37 °C followed by addition of the loading dye containing 25% bromophenol blue, 0.25% xylene cyanol, 30% glycerol (3 μL). The solution was finally loaded on 0.8% agarose gel containing 1.0 μg mL^{-1} ethidium bromide. Electrophoresis was done in a dark chamber for 2.0 h at 60 V in TAE (Tris-acetate EDTA) buffer. The DNA bands were visualized by UV light, photographed and the intensities of the bands quantified using UVITECH Gel Documentation System. Due corrections were made for the low level of nicked circular (NC) form present in the original SC DNA sample and for the low affinity of ethidium bromide binding to SC DNA compared to the NC and linear forms of DNA [39]. The chemical nuclease activity was performed in dark in the presence of H_2O_2 (4 μL) as an oxidant and glutathione (GSH) as a reducing agent. The mechanistic study was done in presence of different additives such as NaN_3 (1 mmol) and 2,2,6,6-tetramethyl-4-piperidone (TEMP, 1 mmol) as singlet oxygen quenchers, superoxide dismutase SOD (4 units) as superoxide radical scavenger, and DMSO (4 μL), KI (1 mmol) and catalase (4 units) as hydroxyl radical scavengers for light exposed reactions. The observed error in measuring the band intensities ranged within 2–5%.

3. Results and discussion

3.1. Synthesis and general aspects

Ligands, namely, tris[(2-*pyridyl*)*methyl*]amine (L^1), N,*N*-bis(2-pyridylmethyl)-N-(2-hydroxybenzyl)amine (HL^2) and N,*N*-dimethyl-N',N'bis(4,6-ditertiarybutyl-2-hydroxybenzyl)ethylenediamine (H_2L^3) were synthesized by literature procedures [33–35]. The ternary iron(II) and iron(III) complexes **1–3** of curcumin having tetradentate charge neutral NNNN–, monoanionic NNNO– and dianionic NNOO-donor ligands were synthesized in good yields and the ligands were found to stabilize iron in its different oxidation states (Fig. 1). The complexes were prepared following a general method by treating the metal chloride salt with the ligand in the first step and the isolated intermediate was further treated with monoanionic curcumin in its methanolic solution. The complexes were characterized from analytical and physicochemical data (Table 1). The mass spectra of the complexes in methanol showed molecular ion peak for **1** and **2** corresponding to the species $[M-Cl]^+$ and the peak for the charge neutral complex **3** corresponded to the species $[M+Na]^+$. The iron(II) complex **1** and the iron(III) complex **2** behaved as 1:1 electrolytes with respective molar conductance value of 58 and 56 S m^2 M^{-1} in DMF, and 114 and 93 S m^2 M^{-1} in 1:1 (v/v) aq. DMF at 25 °C. Complex **3** was non-electrolytic with molar conductance value of ~3 S m^2 M^{-1} in DMF and ~5 S m^2 M^{-1} in 1:1 (v/v) aq. DMF solution at 25 °C. The solid state magnetic susceptibility data at room temperature revealed that the complexes are paramagnetic with a high-spin state for the $3d^6$ Fe(II) (μ_{eff} ~ 5.5 μ_B) in complex **1** and high-spin state of $3d^5$ Fe(III) for the complexes **2** and **3** with a μ_{eff} value of ~5.8 μ_B. The iron(II) complex **1** has a $t_{2g}^4e_g^2$ electronic configuration with four unpaired electrons and

Table 1
Selected Physicochemical Data for the Complexes **1–3.**

Complex	1	2	3
IR[a]/cm^{-1} (C═O str.)	1593	1593	1593
λ_{max}/nm (ε/M^{-1} cm^{-1})[b]	410 (33700)	428 (22200)	425 (17960)
λ_{em}[c]/nm (Φ_F)	530 (0.02)	527 (0.03)	526 (0.02)
E_f[d]/V	0.27[e]	−0.35[f]	−0.37[f]
Λ_M[g]/S m^2 M^{-1}	58	56	3
μ_{eff}[h]/μ_B	5.49	5.52	5.83
K_b[i]/M^{-1}	4.4 (± 0.3) × 10^4	6.3 (± 0.4) × 10^4	5.9 (± 0.6) × 10^4

[a] In solid phase.
[b] In 1:1 DMF/DPBS buffer (pH 7.2, 25 °C).
[c] In DMSO; λ_{ex} = 420 nm (fluorescence quantum yield with respect to fluorescein with a Φ_F = 0.79 in 0.1 M NaOH).
[d] In 5 mL of DMF with 0.1 M TBAP and 2.0 mM complexes. The formal potentials (E_f) were vs. SCE at a scan rate of 50 mV s^{-1}.
[e] Anodic peak potential.
[f] Cathodic peak potential without any anodic counterpart.
[h] $Hg[Co(SCN)_4]$ as standard.
[g] Molar conductivity in DMF.
[i] Intrinsic ct-DNA binding constant (ct, calf thymus).

significant orbital contributions thus giving a magnetic moment that is more than the spin-only value, while it is $t_{2g}^3e_g^2$ for the iron(III) complexes with expected spin-only magnetic moment value. The magnetic data are of importance as high-spin iron(II) species are known to be involved in several enzymatic dioxygen activation reactions and for the activity of anticancer drug bleomycins and its structural mimics [41]. The FT-IR spectra in the solid phase of the complexes **1–3** showed characteristic strong C═O and C═C (β-diketonate) stretching bands near 1593 and 1485 cm^{-1} respectively. Free curcumin in the solid phase showed intense C═O and C = C stretching bands near 1600 and 1505 cm^{-1} respectively [42]. The red shift in these characteristic peaks suggests the enolate form of curcumin bonded to iron in a bidentate fashion. The electronic spectra of the complexes in 1:1 (v/v) DMF/DPBS solution showed a visible band at ~420 nm which was assigned to the curcumin-based transition. Absorption band near 500 nm for complex **1** was assigned to the MLCT (metal to ligand charge transfer) transition which is characteristic of the Fe(II) with π-acceptor polypyridyl ligands [43]. Complexes **2** and **3** showed LMCT (ligand to metal charge transfer) band near 510 nm due to the presence of π -donor phenolate ligands attached to Fe(III) ion [44]. The absorption band in the UV region are due to ligand centered n-π * and π-π * transitions involving the aromatic rings. The emission spectra of the complexes showed a broad band at ~530 nm in DMSO characteristic of the curcumin dye (Fig. 2). The fluorescence quantum yield (Φ_F) of the curcumin ligand alone is reported as 0.06 in DMSO [45]. Upon binding to the paramagnetic iron center, the emission intensity of curcumin got diminished due to the presence of low lying d-d states that quench the fluorescence of the ligand [46]. The Φ_F values of the complexes **1–3** were found to be 0.02, 0.03 and 0.02, respectively. Cyclic voltammogram of the iron(II) complex **1** showed a quasi-reversible oxidative response corresponding to the Fe(III)-Fe(II) redox couple at 0.27 V vs. SCE in DMF-0.1 M TBAP indicating susceptibility of the complex toward oxidation forming the Fe(III) state. The iron(III) complexes **2** and **3** showed an irreversible voltammogram near −0.35 and −0.37 V (versus saturated calomel electrode, SCE) assignable to the reduction of Fe(III) to Fe(II). As these reduction potentials are near the biological redox potentials of reducing thiols, namely, glutathione (GSH), ranging within −0.16 to −0.26 V (versus standard hydrogen electrode), the iron(III) complexes in a hypoxic cellular medium could get reduced to the cytotoxic Fe(II) complexes [47]. The NNOO-donor ligand in complex **3** is found to impart marginally higher redox stability to Fe(III) than the NNNO-donor ligand in complex **2**. This is ascribed to the oxophilic nature of the ferric ion. The tetradentate ligands with

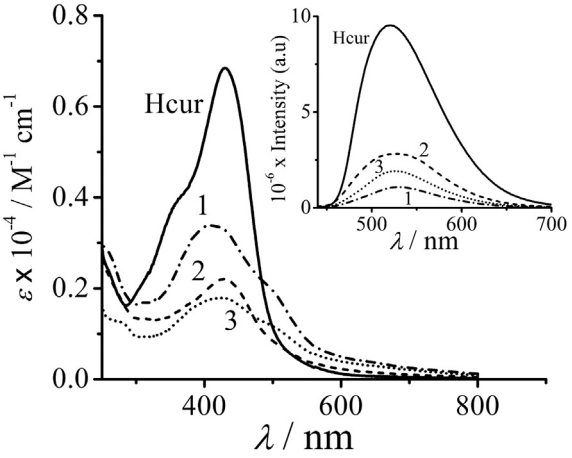

Fig. 2. Electronic absorption spectra of the complexes **1–3** and curcumin in 1:1 (v/v) DMF/DPBS solution. The inset shows the emission spectra of **1–3** and curcumin in DMSO (λ_{ex} = 420 nm).

different numbers of N- and O-donor sites could play an important role in stabilizing the metal in different oxidation states in the ternary structures.

3.2. Solution stability

Curcumin has low aqueous solubility and poor bioavailability due to hydrolytic instability causing its rapid degradation in aqueous media with a short half-life of 20 min at pH 7.4 [22]. The metal complexes of curcumin are known to stabilize curcumin under physiological conditions even after 48 h in the dark [22]. The iron(II/III) complexes **1–3** showed significant solution stability in the dark as evidenced from the UV–visible spectral measurements in 1:1 DMSO/Tris-HCl buffer (pH 7.2 at 37 °C). Complex **1** having high-spin Fe(II) in a $Fe^{II}N_4O_2$ core is comparatively less stable among the three. Stability of charge neutral complex **3** with a $Fe^{III}N_2O_4$ core is more than complex **2** with a $Fe^{III}N_3O_3$ core. The presence of more O-donor sites seems to have stabilizing effect due to the oxophilicity of iron(III). Again, the complexes showed better stability than curcumin alone under photo-irradiated conditions.

3.3. Theoretical studies

Density functional theory (DFT) was used to derive the computed structures of the complexes **1–3** for rationalization of their structural and spectral aspects using B3LYP and Lanl2DZ basis sets with Gaussian programs [36,37]. The optimized structures along with the HOMO−-LUMO energy levels are shown in Fig. 3. From the frontier molecular orbital (FMO) pictures it is evident that HOMO for complexes **1** and **2** is located over the curcumin moiety with less contribution of the metal and other ancillary ligand, while for complex **3** it is located over the ancillary ligand. The LUMO for all the complexes is located over the curcumin moiety only. Two M−O(cur) distances are 1.99, 2.03 Å for **1**; 1.99, 1.96 Å for **2**; and 2.01, 2.13 Å for **3**. Energy difference between the LUMO and HOMO of the complexes are 3.07, 2.88 and 2.75 eV for complexes **1–3**, respectively. The optimized coordinates were used for further calculations and optimization of the excited state geometry which showed an increase in the M−O(cur) bond length which is significant for complex **3** compared to other two complexes. This predicts for facile photo-induced release of curcumin from complex **3**.

3.4. Glutathione dependent release of curcumin

Stability of the complexes in presence of biological reducing agent glutathione (GSH) was studied by monitoring the fluorescence intensity of the complexes over a period of 1 h. To prevent any degradation of the released curcumin, DMSO solution of complexes **1–3** (20 μM) was used with 1 eq. of glutathione (Fig. 4). Complex **2** having a reduction potential within the biological potential window showed maximum release of curcumin via reduction of Fe(III) to Fe(II). A lower extent of curcumin release from complex **3** in comparison to complex **2** is related to their redox potentials showing relatively higher stabilization of Fe (III) in **3** than in **2**. A relatively small change in the emission intensity of complex **1** over the time period used indicates less displacement of curcumin from the metal in its reduced +2 oxidation state giving an order for curcumin release as: **2** ($Fe^{III}N_3O_3$ core) > **3** ($Fe^{III}N_2O_4$ core) > > **1** ($Fe^{II}N_4O_2$ core).

3.5. Photo-release of curcumin

The metal–ligand bond lengths are expected to elongate in the excited states of the transition metal complexes thus making ligand release more facile as well as selective [1,48]. To explore such a possibility for these complexes, DMSO solutions of the complexes were photo-irradiated with the visible light of 400–700 nm using a photoreactor, and the corresponding changes in the fluorescence spectra were monitored in different time intervals (Fig. 4). Photo-irradiation caused a steady increase in the emission intensity of curcumin indicating release of the dye from the paramagnetic complexes compared to the intensity of its counterpart kept in dark and used as a control. Complex **3** showed maximum release of curcumin as theoretical studies shown that the Fe—O bond length in complex **3** is longer compared to those in complexes **1** and **2** in their excited states. The emission after certain time gap got saturated or decreased due to expected degradation of the free curcumin in presence of photo-generated reactive oxygen species (ROS). This observation is of significance as selective delivery of curcumin inside the cancer cells and activation via photo- irradiation with visible light is of importance in anticancer drug development. The photo-release of curcumin from its complexes follows the order: **3** ($Fe^{III}N_2O_4$ core) > > **1** ($Fe^{II}N_4O_2$ core) ≥ **2** ($Fe^{III}N_3O_3$ core). Besides the electronic effect, steric effect is more pronounced in the structure of complex **3** facilitating the ligand release (Fig. 1).

3.6. Photocytotoxicity in visible light

The anti-proliferative activity of the complexes **1–3** to inhibit cellular growth and induce cell death upon irradiation with visible light (400–700 nm) in MCF-7 (breast carcinoma), LN-229 (human glioblastoma) and HaCaT (human skin keratinocyte) cell lines was investigated using MTT (3-(4,5-dimethylthiazol-2-yl)-2,5-diphenyltetrazolium bromide) assay. The complexes **2** and **3** were essentially non-toxic in dark in LN-229 and HaCaT cells giving IC_{50} values of > 90 μM, while the same for MCF-7 were ~54 and ~45 μM indicating minor dark cytotoxicity. These two complexes, however, showed significant light-induced cytotoxicity in all three cell lines with IC_{50} values ranging within 7–21 μM. The activity of the iron(III) complexes seems to result from light induced conversion from Fe(III) to Fe(II) for ROS generation. Complex **1** having iron(II), in contrast, showed similar moderate toxicity in both light and dark with the IC_{50} values ranging within 6–18 μM in all three cells. The light effect was not apparent for MCF-7, while a marginal photocytotoxicity was observed for the other two cell lines used. The dark toxicity for complex **1** could be attributed to the high spin +2 oxidation state of the metal and low value of Fe(III)-Fe(II) redox couple, that could result in the generation of ROS from dioxygen activation in a similar way that is known for bleomycins in an oxygenated medium [27]. The effect of light was thus not observed for the metal in its reduced oxidation state. Table 2 lists the IC_{50} values of the complexes **1–3** along with few reported iron complexes [49–51]. While iron(III) complexes are generally more photoactive than the iron(II) complexes, the high spin iron(II) complexes, in contrast, show significant activity as chemotherapeutic agents like bleomycins and its

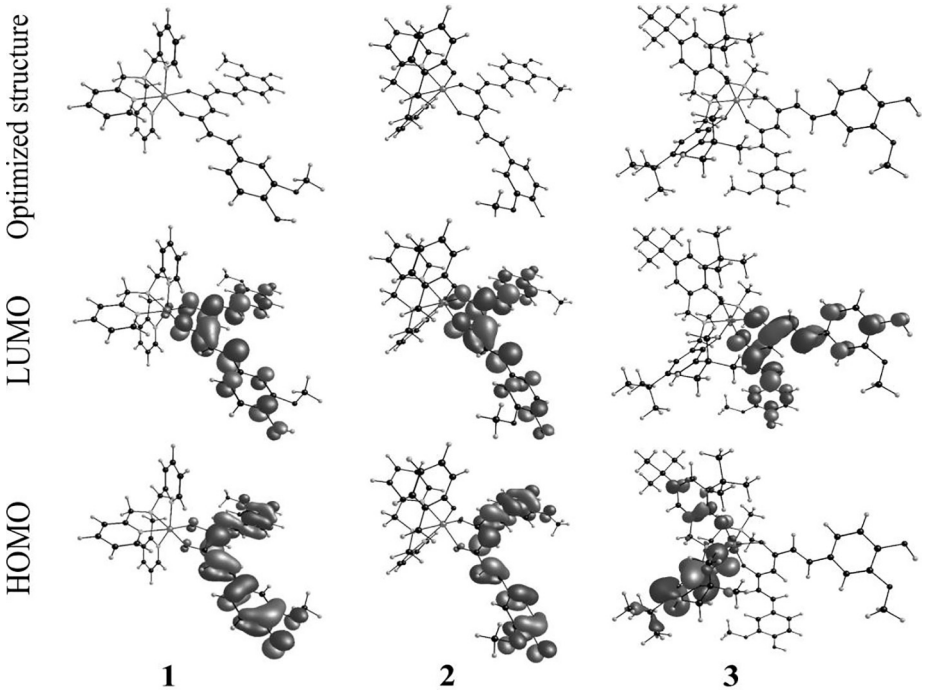

Fig. 3. The optimized structures and frontier molecular orbitals (FMOs) of the complexes **1–3**. (For interpretation of the references to colour in this figure legend, the reader is referred to the web version of this article.)

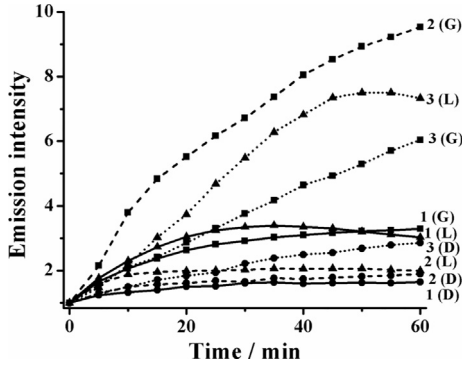

Fig. 4. A comparison of the fluorescence intensities of the complexes **1–3** (20 μM in DMSO) in the dark (D), in visible light of 400–700 nm (L, 10 J cm^{-2}), and with one eq. of glutathione (GSH) for a period of 1 h.

analogues [27,51]. The complexes with light-induced cytotoxicity are potentially suitable as drug (e.g. curcumin) carrier releasing the drug on chemical or photochemical activation.

3.7. Cellular localization

The fluorescent curcumin moiety in the complexes has enabled us to study the cellular localization of the complexes **1–3**. The HaCaT cells were incubated with the complexes (15 μM) for 4 h in dark and subjected for confocal microscopy study. Hoechst dye was used as a nuclear staining agent. After 4 h of incubation, the complexes showed no nuclear localization. When mito-tracker red (MTR) was used as mitochondria staining dye, the complexes showed preferential localization in the mitochondria of the HaCaT cells as evident from the merge images of MTR and the complexes (Fig. 5). Mitochondria being the powerhouse of the cell and DNA repair mechanism being absent in the mitochondria, any mitochondrial dysfunction results in apoptotic cell death via caspases signaling. Complexes **1–3** are thus of significance as potential mitochondria-targeting drug releasing agents [52,53].

Table 2
IC_{50} values[a,b] (μM) of **1–3** and related iron complexes.[c–f]

Cell Type	$[Fe(L^1)(cur)]Cl$ (**1**)	$[Fe(L^2)(cur)]Cl$ (**2**)	$[Fe(L^3)(cur)]$ (**3**)	Curcumin
MCF-7 (Light)	14.2 (± 1.2)	10.3 (± 1.2)	12.8 (± 1.8)	7.4 (± 0.7)
MCF-7 (Dark)	15.9 (± 1.5)	52.4 (± 3.4)	44.9 (± 3.1)	15.1 (± 1.2)
LN-229 (Light)	8.8 (± 0.9)	11.3 (± 1.1)	14.4 (± 1.7)	5.4 (± 0.6)
LN-229 (Dark)	20.3 (± 1.9)	90.1 (± 5.6)	> 100	8.7 (± 1.2)
HaCaT (Light)	6.6 (± 0.8)	7.1 (± 0.6)	20.7 (± 2.1)	2.5 (± 0.5)
HaCaT (Dark)	18.1 (± 2.1)	> 100	> 100	13.9 (± 1.3)

[a] In 2% dimethyl sulfoxide culture media. MCF-7 cell is human breast carcinoma, LN-229 is human glioblastoma cell and HaCaT is human skin keratinocyte.

[b] Light of 400–700 nm (Luzchem photoreactor).

[c] $[Fe(Hqpy)(CH_3CN)_2](ClO_4)_2$ [51]: IC_{50} (μM) in light [dark] in HeLa cells = 4 [> 100], where ligand Hqpy is 2,2′:6′,2″:6″,2‴:6‴,2⁗-quinquepyridine.

[d] $[Fe(Phqpy)(CH_3CN)_2](ClO_4)_2$ [51]: IC_{50} (μM) light [dark] in HeLa cells = 7.74 [> 100].

[e] $[Fe(BHA)(pydpa)Cl]Cl{\cdot}H_2O$ [50]: IC_{50} (μM) light [dark] in HeLa cells = 14.6 [77], where BHA and pydpa are benzhydroxamate and (pyrenyl) dipicolylamine respectively.

[f] [FeL(dppzCB)] [49]: IC_{50} (μM) light [dark] in HepG2 cells = 7.8 [15.1] and ligand dppzCB is 2-((2-biotinamido)ethyl) amidodipyrido[3,2-*α*:2′,3′-*c*]-phenazine.

3.8. DNA binding and cleavage

Since confocal imaging showed mitochondrial (mt) localization of the complexes, mtDNA could be a target of the complexes for the cellular activity. The interaction of the complexes with calf thymus DNA (ct-DNA) was studied by UV–Visible absorption titration experiment. The intrinsic ct-DNA binding constant (K_b) values for the complexes were $\sim 10^4\,M^{-1}$ in 5% DMF-Tris buffer (pH = 7.2) suggesting partial intercalative mode of DNA binding giving an order: **2** > **3** > **1** (Table 1) [54]. The photo-induced DNA cleavage activity of the

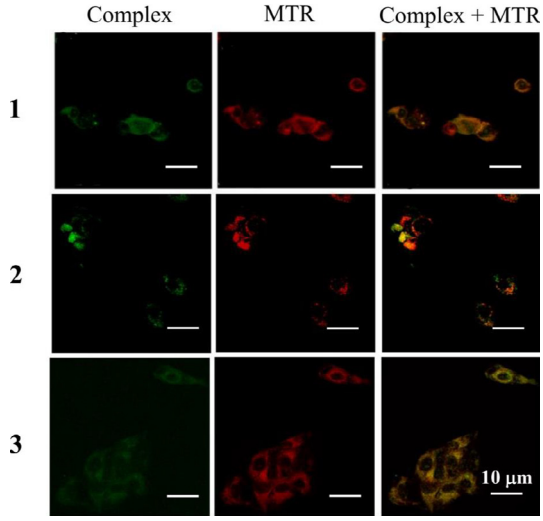

Fig. 5. Confocal microscopy images of the complexes **1–3** in HaCaT cells recorded after 4 h of incubation using MitoTracker Deep Red (MTR) as the staining agent for mitochondria (scale bar: 10 μm).

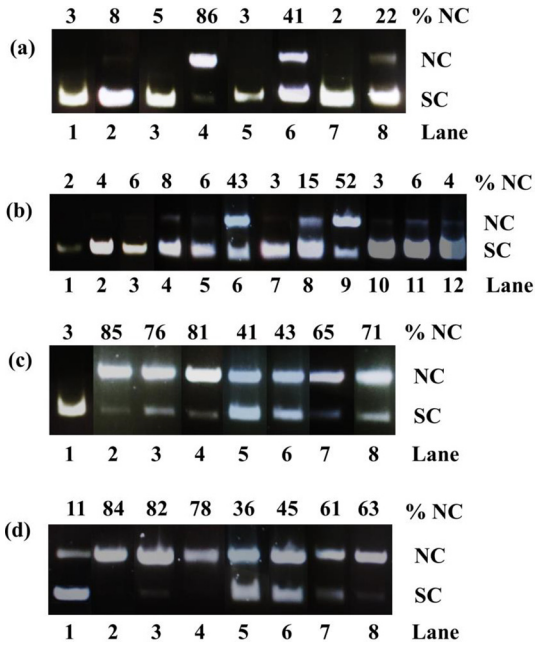

Fig. 6. Gel electrophoresis diagram showing (a) the visible light-induced DNA cleavage activity of 20 μM complexes **1–3** at 446 nm (50 mW diode laser) using SC pUC19 DNA (0.2 μg, 30 μM) for an exposure time of 1 h: lane-1, DNA control (D); lane-2, DNA control (L); lane-3, DNA + **1** (D); lane-4, DNA + **1** (L); lane-5, DNA + **2** (D); lane-6, DNA + **2** (L); lane-7, DNA + **3** (D); lane-8, DNA + **3** (L) [D, in dark; L, in light]. (b) Chemical nuclease activity in dark for 2 h incubation: lane-1, DNA control; lane-2, DNA + glutathione (GSH); lane-3, DNA + H_2O_2; lane-4, DNA + **1**; lane-5, DNA + **1** + GSH; lane-6, DNA + **1** + H_2O_2; lane-7, DNA + **2**; lane-8, DNA + **2** + GSH; lane-9, DNA + **3** + H_2O_2; lane-10, DNA + **3**; lane-11, DNA + **3** + GSH; lane-12, DNA + **3** + H_2O_2. Mechanistic study using the complex (**C**) (**1** in (c) and **2** in (d); D, in dark; L, in light) and SC pUC19 DNA (0.2 μg, 30 μM): lane-1, DNA + **C** (D); lane-2, DNA + **C** (L); lane-3, DNA + **C** + TEMP (L); lane-4, DNA + **C** + NaN_3 (L); lane-5, DNA + **C** + KI (L); lane-6, DNA + **C** + DMSO (L); lane-7, DNA + **C** + catalase (L); lane-8, DNA + **C** + SOD (L).

complexes was studied using supercoiled (SC) pUC19 DNA (30 μM, 0.2 μg) in Tris–HCl/NaCl (50 mM, pH = 7.2) buffer by taking 20 μM concentration of each sample along with the dark controls (Fig. 6). The agarose gel electrophoresis was done to assess the extent of nicked circular (NC) DNA formation from the SC DNA in presence of the complexes. Monochromatic visible light source of 446 nm (50 mW power) was used from a continuous-wave (CW) diode laser. The wavelength chosen for the DNA photocleavage activity is based on the presence of an absorption band near 430 nm wavelength. Each sample (20 μM), after treating with the DNA solution in Tris–HCl buffer medium, was incubated for 1 h in the dark. Complexes **1–3** gave respective 86, 41 and 22% of NC DNA under similar experimental conditions. For the mechanistic study of ROS generation, complexes **1–3** were treated with pUC-19 DNA and photo-exposed in presence of different singlet oxygen quenchers (TEMP, NaN_3), hydroxyl radical scavengers (KI, DMSO and catalase), and SOD as superoxide radical scavenger. The iron(II) complex **1** in presence of H_2O_2 showed significant DNA cleavage activity in dark following the Fenton-type mechanism and this also accounted for the dark cytotoxicity of the complex in LN-229 cells observed from the MTT assay [55]. The iron(III) complex **2** also showed DNA cleavage in presence of H_2O_2 as iron(III) could catalyze decomposition of H_2O_2 forming hydroxyl radical, whereas iron (III) complex **3** was found to be inactive in the presence of H_2O_2 with less susceptibility of the metal in getting reduced. Complexes **1–3** did not show any significant DNA cleavage activity in the presence of reducing agent glutathione (GSH). The complexes in presence of hydroxyl radical scavengers showed low DNA photocleavage activity. No suppressed activity was observed in presence of other ROS quenchers/scavengers. The complexes thus solely generated hydroxyl radicals as the ROS on exposure to light resulting in the photo-activated anticancer activity.

4. Conclusions

Iron complexes of curcumin with the metal in its +2 and +3 oxidation states and having three different ancillary ligands with NNNN–, NNNO– and NNOO-binding sites are prepared to explore their curcumin releasing properties by chemical and photochemical means using glutathione as a reducing agent or visible light (400–700 nm) as an activator. The neutral NNNN-donor ligand stabilized iron(II) in its high spin with $t_{2g}^4e_g^2$ electronic configuration, while monoanionic NNNO– and dianionic NNOO-donor ancillary ligands stabilized high spin iron(III) with $t_{2g}^3e_g^2$ configuration in these pseudo-octahedral complexes. The spectral, redox and biological properties of the complexes were used for deriving a structure–activity relationship. The sterically encumbered iron(III) complex **3** showed significant curcumin release on light activation giving an order: **3** ($Fe^{III}N_2O_4$ core) > > **1** ($Fe^{II}N_4O_2$ core) ≥ **2** ($Fe^{III}N_3O_3$ core), while the effect was less pronounced in the presence of glutathione as a reducing agent for the iron(III) complexes giving an overall order: **2** > **3** > > **1**. The efficacy of curcumin release was analysed from the redox properties and the DFT data on excited state structures. The complexes showed moderate photo-cytotoxicity in MCF-7 breast carcinoma, LN-229 human glioblastoma and HaCaT keratinocyte cells in visible light. Stabilization of curcumin on binding to the metal ion and release it from the iron centre accounts for observed moderately high IC_{50} values of the metal complexes. The high-spin iron (II) complex **1** showed some dark toxicity with an IC_{50} value of ~20 μM, while the iron(III) complexes are essentially non-toxic (IC_{50}: > 90 μM for **2** and **3** respectively) in the dark in LN-229 cells. In other two cell lines also IC_{50} values are similar. The iron complexes are thus suitable candidates for cellular delivery of curcumin as a drug. Mechanistic study on the photocleavage of pUC19 DNA showed formation of hydroxyl radicals as the reactive oxygen species with the metal ion in different oxidation states playing important roles based on their redox properties. A Fenton-type mechanism seems to be operative as is known for the anticancer activity of iron-bleomycins. An important observation of this study is the mitochondrial localization of the complexes with mitochondrial DNA as the possible target instead of nuclear DNA for which the nuclear excision repair (NER) mechanism exists for deactivating the drug. The results showed the importance of the

ancillary ligand in stabilizing iron in different redox states and on the overall activity of the complexes. Significant drug release from the iron curcumin conjugates could be achieved by photochemical means for potential photo-chemotherapeutic applications. This work presents further scope of designing new iron conjugates for selective cellular delivery of metal-bound chemotherapeutic drugs using light as an activator.

Acknowledgements

We thank the Department of Science and Technology (DST), Government of India, for the financial support (DST/SR/S5/MBD-02/2007, EMR/2015/000742). A.R.C. thanks the DST for J.C. Bose national fellowship. A.J. and A.G. are thankful to IISc and BIRAC SRISTI for their respective research fellowship. We thank the Alexander von Humboldt Foundation for donation of an electro-analytical system.

Appendix A. Supplementary data

ESI-MS (Figs. S1–S3), IR spectral plots (Figs. S4–S6), cyclic voltammograms (Fig. S7–S9), UV-visible spectra (Fig. S10), emission spectra (Fig. S11), MTT assay plots in different cell lines (Fig. S12, S13), confocal imaging (Fig. S14), DNA binding plots (Fig. S15), structural parameters from theoretical studies (Tables S1–S4) and bond parameter table from the theoretical studies (Table S5). Supplementary data associated with this article can be found, in the online version, at https://doi.org/10.1016/j.ica.2018.09.008.

References

[1] A.K. Renfrew, Metallomics 6 (2014) 1324–1335.
[2] R. Mahato, W. Tai, K. Cheng, Adv. Drug Deliv. Rev. 63 (2011) 659–670.
[3] G. Manish, S. Vimukta, J. Chem. Sci. 1 (2011) 135–138.
[4] S.R. Mchinney, R.M. Goldberg, H.L. McLeod, Mol. Cancer Ther. 8 (2010) 10–16.
[5] A.-M. Florea, D. Büsselberg, Cancers (Basel) 3 (2011) 1351–1371.
[6] K. Barabas, R. Milner, D. Lurie, C. Adin, Vet. Comp. Oncol. 6 (2008) 1–18.
[7] T. Iwamoto, Biol. Pharm. Bulliten 36 (2013) 715–718.
[8] A. Duvoix, R. Blasius, S. Delhalle, M. Schnekenburger, F. Morceau, E. Henry, M. Dicato, M. Diederich, Cancer Lett. 223 (2005) 181–190.
[9] K. Rashid, S. Chowdhury, S. Ghosh, P.C. Sil, Biochem. Pharmacol. 143 (2017) 140–155.
[10] B. Aggarwal, K. Harikumar, Int. J. Biochem. Cell Biol. 41 (2009) 40–59.
[11] K.I. Priyadarsini, Molecules 19 (2014) 20091–20112.
[12] D. Mathew, W.L. Hsu, J. Funct. Foods 40 (2018) 692–699.
[13] P. Brennan, L.A.J. O'Neill, Biochem. Pharmacol. 55 (1998) 965–973.
[14] T. Esatbeyoglu, P. Huebbe, I.M.A. Ernst, D. Chin, A.E. Wagner, G. Rimbach, Angew. Chemie – Int. Ed. 51 (2012) 5308–5332.
[15] J.B. Baell, J. Nat. Prod. 79 (2016) 616–628.
[16] K.M. Nelson, J.L. Dahlin, J. Bisson, J. Graham, G.F. Pauli, M.A. Walters, J. Med. Chem. 60 (2017) 1620–1637.
[17] W.-H. Lee, C.-Y. Loo, M. Bebawy, F. Luk, R. Mason, R. Rohanizadeh, Curr. Neuropharmacol. 11 (2013) 338–378.
[18] A. Sahu, N. Kasoju, U. Bora, Biomacromolecules 9 (2008) 2905–2912.
[19] A. Surís, J. Smith, C. Powell, C.S. North, Ann. Clin. Psychiat. 25 (2013) 33–40.
[20] F. Harris, L. Pierpoint, Med. Res. Rev. 29 (2012) 1292–1327.
[21] S. Banerjee, I. Pant, I. Khan, P. Prasad, A. Hussain, P. Kondaiah, A.R. Chakravarty, Dalton Trans. 44 (2015) 4108–4122.
[22] A. Garai, I. Pant, S. Banerjee, B. Banik, P. Kondaiah, A.R. Chakravarty, Inorg. Chem. 55 (2016) 6027–6035.
[23] K. Mitra, S. Gautam, P. Kondaiah, A.R. Chakravarty, Angew. Chemie – Int. Ed. 54 (2015) 13989–13993.
[24] D. Pucci, A. Crispini, B.S. Mendiguchía, S. Pirillo, M. Ghedini, S. Morelli, L. De Bartolo, Dalton Trans. 42 (2013) 9679.
[25] U. Bhattacharyya, B. Kumar, A. Garai, A. Bhattacharyya, A. Kumar, S. Banerjee, P. Kondaiah, A.R. Chakravarty, Inorg. Chem. 56 (2017) 12457–12468.
[26] A.K. Renfrew, N.S. Bryce, T.W. Hambley, Chem. Sci. 4 (2013) 3731.
[27] G. Roelfes, M. Lubben, S.W. Leppard, E.P. Schudde, R.M. Hermant, R. Hage, E.C. Wilkinson, L. Que, B.L. Feringa, J. Mol. Catal. A Chem. 117 (1997) 223–227.
[28] J.B. Neilands, J. Biol. Chem. 270 (1995) 26723–26726.
[29] K.N. Raymond, E.A. Dertz, S.S. Kim, Proc. Natl. Acad. Sci. 100 (2003) 3584–3588.
[30] S.M. Khopde, K.I. Priyadarsini, D.K. Palit, T. Mukherjee, Photochem. Photobiol. 72 (2000) 625–631.
[31] M. López-Lázaro, Mol. Nutr. Food Res. 52 (2008) 103–127.
[32] C. Eaborn, J. Organomet. Chem. 213 (1981) C62.
[33] A. Beni, A. Dei, S. Laschi, M. Rizzitano, L. Sorace, Chem. – A Eur. J. 14 (2008) 1804–1813.
[34] E.Y. Tshuva, I. Goldberg, M. Kol, Z. Goldschmidt, Inorg. Chem. 40 (2001) 4263–4270.
[35] R. Mayilmurugan, K. Visvaganesan, E. Suresh, M. Palaniandavar, Inorg. Chem. 48 (2009) 8771–8783.
[36] (a) W.R. Wadt, P.J. Hay, J. Chem. Phys. 82 (1985) 284–298;
(b) A.D. Becke, Phys. Rev. A 38 (1988) 3098–3100.
[37] Gaussian 16, Revision B.01, M.J. Frisch, G.W. Trucks, H.B. Schlegel, G.E. Scuseria, M.A. Robb, J.R. Cheeseman, G. Scalmani, V. Barone, G.A. Petersson, H. Nakatsuji, X. Li, M. Caricato, A.V. Marenich, J. Bloino, B.G. Janesko, R. Gomperts, B. Mennucci, H.P. Hratchian, J.V. Ortiz, A.F. Izmaylov, J.L. Sonnenberg, D. Williams-Young, F. Ding, F. Lipparini, F. Egidi, J. Goings, B. Peng, A. Petrone, T. Henderson, D. Ranasinghe, V.G. Zakrzewski, J. Gao, N. Rega, G. Zheng, W. Liang, M. Hada, M. Ehara, K. Toyota, R. Fukuda, J. Hasegawa, M. Ishida, T. Nakajima, Y. Honda, O. Kitao, H. Nakai, T. Vreven, K. Throssell, J.A. Montgomery, Jr., J.E. Peralta, F. Ogliaro, M.J. Bearpark, J.J. Heyd, E.N. Brothers, K.N. Kudin, V.N. Staroverov, T.A. Keith, R. Kobayashi, J. Normand, K. Raghavachari, A.P. Rendell, J.C. Burant, S.S. Iyengar, J. Tomasi, M. Cossi, J.M. Millam, M. Klene, C. Adamo, R. Cammi, J.W. Ochterski, R.L. Martin, K. Morokuma, O. Farkas, J.B. Foresman, and D.J. Fox, Gaussian, Inc., Wallingford CT, 2016.
[38] T. Mosmann, J. Immunol. Methods 65 (1983) 55–63.
[39] S. Roy, A.K. Patra, S. Dhar, A.R. Chakravarty, Inorg. Chem. 47 (2008) 5625–5633.
[40] R.P. Paitandi, S. Mukhopadhyay, R.S. Singh, V. Sharma, S.M. Mobin, D.S. Pandey, Inorg. Chem. 56 (2017) 12232–12247.
[41] E.B. Meltzer, Am. J. Respir. Cell Mol. Biol. 53 (2015) 748–749.
[42] K. Nakamoto, Infrared and Raman Spectra of Inorganic and Coordination Compounds. Part A, Theory and Applications in Inorganic Chemistry, John Wiley & Sons, 2006.
[43] H. Krass, E.A. Plummer, J.M. Haider, P.R. Barker, N.W. Alcock, Z. Pikramenou, M.J. Hannon, D.G. Kurth, Angew. Chemie - Int. Ed. 40 (2001) 3862–3865.
[44] S. Heidari, E. Safaei, A. Wojtczak, P. Cotič, A. Kozakiewicz, Polyhedron 55 (2013) 109–116.
[45] S. Banerjee, A.R. Chakravarty, Acc. Chem. Res. 48 (2015) 2075–2083.
[46] A. Garai, U. Basu, I. Pant, P. Kondaiah, A.R. Chakravarty, J. Chem. Sci. 127 (2015) 609–618.
[47] K.K. Millie, K.H. Weaver, D.L. Rabenstein, J. Org. Chem. 58 (1993) 4144–4146.
[48] T. Respondek, R.N. Garner, M.K. Herroon, I. Podgorski, C. Turro, J.J. Kodanko, J. Am. Chem. Soc. 133 (2011) 17164–17167.
[49] S. Saha, R. Majumdar, A. Hussain, R.R. Dighe, A.R. Chakravarty, Phil. Trans. R. Soc. A 371 (2013) 20120190-15.
[50] A. Garai, U. Basu, I. Khan, I. Pant, A. Hussain, P. Kondaiah, A.R. Chakravarty, Polyhedron 73 (2014) 124–132.
[51] E.L.-M. Wong, G.-S. Fang, C.-M. Che, N. Zhu, Chem. Commun. (2005) 4578.
[52] S. Banerjee, P. Prasad, I. Khan, A. Hussain, P. Kondaiah, A.R. Chakravarty, Z. Anorg, Allg. Chem. 640 (2014) 1195–1204.
[53] T. Sarkar, S. Banerjee, A. Hussain, RSC Adv. 5 (2015) 16641–16653.
[54] A. Rescifina, C. Zagni, M.G. Varrica, V. Pistarà, A. Corsaro, Eur. J. Med. Chem. 74 (2014) 95–115.
[55] J.P. Kehrer, Toxicology 149 (2000) 43–50.